Multi-Scale Interactions of Microtearing Turbulence in the Tokamak Pedestal

M.J. Pueschel[1,2,3], D.R. Hatch[3], M. Kotschenreuther[3], A. Ishizawa[4], and G. Merlo[3]

[1]*Dutch Institute for Fundamental Energy Research,*

5612 AJ Eindhoven, The Netherlands

[2]*Eindhoven University of Technology,*

5600 MB Eindhoven, The Netherlands

[3]*Institute for Fusion Studies, University of Texas at Austin, Austin, Texas 78712, USA*

[4]*Graduate School of Energy Science,*

Kyoto University, Uji, Kyoto, 611-0011, Japan

Abstract

Microtearing turbulence in an idealized pedestal scenario is found to saturate via zonal fields, while also exciting strong zonal flows; a concurrent upshift of the nonlinear critical gradient is observed. The zonal flows cause electron-temperature-gradient-driven turbulence to be ameliorated. When applying resonant magnetic perturbations, the prompt charge loss off the flux surface erodes the zonal flow, leading to higher electron-scale fluxes, while leaving microtearing saturation physics unaffected.

On the road to fusion energy, the ability to reliably access and control high-performance regimes in magnetic confinement devices is key. One common such means is through H-mode operation [1], where an edge transport barrier called the pedestal is established. While this configuration tends to be unstable to edge-localized modes – which, however, may be mitigated by, e.g., resonant magnetic perturbations (RMPs) [2, 3] – that are associated with the peeling-ballooning instability threshold [4], the overall evolution of the pedestal requires essential contributions from electron microinstabilities [5, 6].

On electron-gyroradius ρ_e scales, electron-temperature-gradient-driven (ETG) turbulence [7] drives electrostatic flux, whereas on ion-sound-gyroradius ρ_s scales, microtearing (MT) modes [8–10] may be destabilized at finite electron pressure β. Both modes exhibit similar transport fingerprints [6, 11, 12], where, unlike for the magnetohydrodynamic ballooning-type instabilities, electron heat diffusivities greatly excede particle diffusivities, a key requirement in explaining pedestal evolution.

Interaction of turbulence across ion-electron scales is commonly studied for electrostatic modes [13–16], whereas the MT-ETG system is less-explored. In Ref. [17], core MT is strongly suppressed by the radial $E \times B$ flow created by the ETG. It is to be stressed, however, that different flavors of MT rely to differing degrees on the electrostatic potential Φ; and as will be shown below, the present MT case is insensitive to background $E\times B$ flow. Another potentially multi-scale mechanism is the impact of RMPs on microturbulence, in particular due to the deleterious effect of resonant shear-magnetic fluctuations $A_\parallel$ on zonal flows [18, 19]: transport from electrostatic ion-scale turbulence can thus be boosted [20–23].

The term *multi-scale* generically refers to the inclusion of multiple spatial or temporal scales in simulations, and is commonly used to refer to the concurrent treatment of ion and electron scales in both space and time simultaneously. Such a treatment is beyond the capacity of present-day computing resources; in the present study, the term multi-scale is taken to refer solely to multiple spatial scales, and arguments will be brought forth why little impact from electron on ion scales is to be expected. Once resolving the full spatio-temporal scales becomes feasible, a direct test of these arguments will be possible.

In order to ensure numerical robustness as well as tractability, an idealized pedestal scenario is created based on DIII-D discharge #98889 [24], where spectrograms have revealed clear MT features and for which gyrokinetic analysis has demonstrated essential contributions from MT turbulence [6, 25]. A local flux tube based on circular flux surfaces [26]

is used at normalized radius $r/a = 0.9725$. As the following analyses cover toroidal mode numbers as low as $n = 4$, even though saturated turbulent amplitudes peak at higher n, it is to be pointed out that the assumptions underlying local flux tubes begin to break down at low n, where the radial variation of profiles between rational surfaces can become significant. Radially global simulations [12] are a possible solution but require significantly more computational effort. Experimental parameters are matched approximately: the normalized electron temperature and density gradients are $a/L_T = 60$ and $a/L_n = 25$, respectively, the safety factor $q_0 = 4.43$, the normalized magnetic shear $\hat{s} = 0.532$, the trapped fraction $\epsilon_\mathrm{t} = 0.437$, the Debye length $\lambda_\mathrm{D} = 0.0222$ normalized to ρ_s, and $\beta = 0.00105$. A Landau collision operator is used with the dimensionless collision frequency $\nu_\mathrm{c} = 0.0024$, equivalent $\nu_\mathrm{ei} = 0.576$ in standard normalized frequency units; ions are assumed to be adiabatic, using deuterium mass ratio for normalization purposes. As ion-scale electrostatic instabilities are thus removed, no background $E \times B$ shear was included. With this setup, saturated turbulence at different scales can straightforwardly be achieved, and the circular geometry allows for clean mode parity identification.

It is to be stressed that even with adiabatic ions, MT instability still occurs at what – given the assumed mass ratio – would be ion scales, and the present results would similarly apply to a kinetic-ion system. Therefore, throughout this paper, the term *ion scales* is used to refer to the range of wavenumbers unstable to MT, even though technically, a vastly different choice of mass ratio would result in this range no longer corresponding to the actual ion scales.

Numerical settings for nonlinear multi-scale simulations with the gyrokinetic [27] turbulence code GENE [28] (see Ref. [29] for the governing equations) are $(2048, 1536, 24, 32, 8)$ grid points along the $(x, y, z, v_\parallel, \mu)$ coordinates, referring respectively to the radial (box size $51.2\rho_\mathrm{s}$), binormal (lowest toroidal mode number $n = 4$, corresponding to $k_y = 0.367$), and parallel direction, as well as to parallel velocity and magnetic moment. Fourth-order hyperdiffusion [30] settings are $D_z = 20$, with additional $D_x = 0.05$ and $D_y = 0.75$ for ion-scale simulations—the latter settings avoid low-k_y ETG excitation but does not impact MT too strongly. Otherwise, single-scale simulations differ from multi-scale runs merely by the resolved range of toroidal mode numbers and corresponding y and x resolutions. Numerical convergence with respect to resolutions and hyperdiffusion was ensured separately for ion- and electron-scale fluxes.

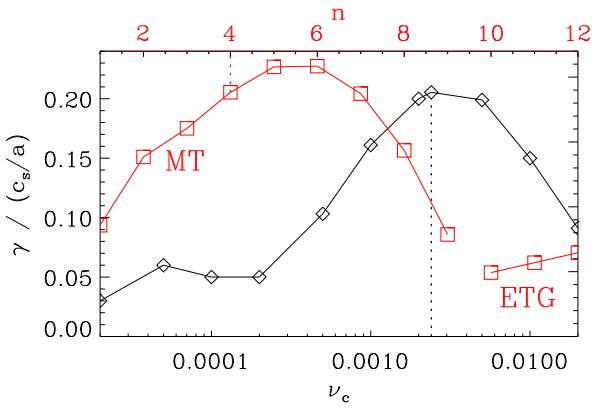

FIG. 1. Growth rates γ as functions of ν_c ($n = 4$, black diamonds) and toroidal mode number (red squares). MT growth peaks near the default collisionality (dotted black line). Modes are centered at zero ballooning angle.

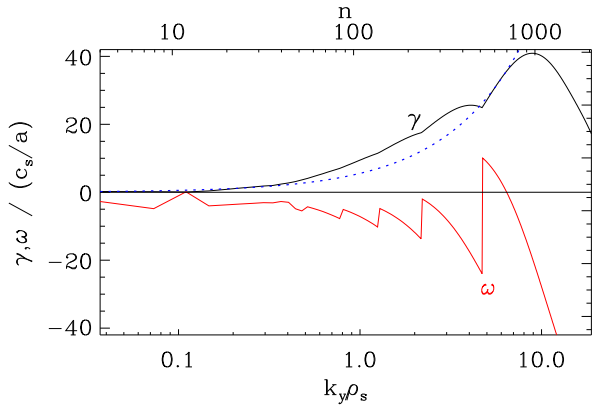

FIG. 2. Growth rate (black) and frequency (red) spectra across all scales. The first two points ($n = 4, 8$) are MT, the remainder various ETG branches. A dotted blue line indicates linear scaling $\gamma \propto k_y$. See Fig. 1 for more clearly discernible MT growth rates at the lowest n.

Linearly, as seen in Fig. 1, MT is unstable at mode numbers $n \leq 9$, and while a collisionless MT branch exists, the default ν_c produces a semi-collisional mode; note that the growth rate γ changes by only $\sim 10\%$ when zeroing out Φ. In this respect, the present MT more closely resembles the mode described in Ref. [31] than that in Ref. [32]. Here, the MT is destabilized by a/L_T, with a/L_n stabilizing at $n = 8$ but not affecting $\gamma(n = 4)$. The default β lies well above the MT stability threshold of 0.02%.

Figure 2 illustrates the instability across scales, with only the first two points ($n = 4, 8$)

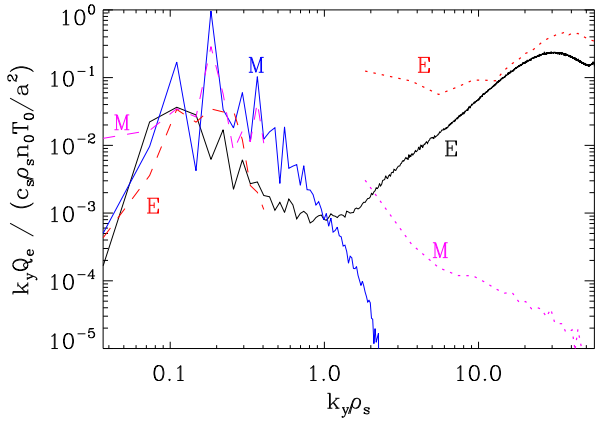

FIG. 3. Heat fluxes multiplied by k_y from multi-scale (solid lines) and single-scale (dashed: ion, dotted: electron) simulations. Letters indicate electrostatic (E, black/red) and magnetic (M, blue/pink) flux channels. Small deviations between ion-scale and multi-scale Q_e result from limited temporal statistics, whereas the decrease in electron-scale Q_e^es is due to multi-scale interaction.

being MT, the remainder various flavors of ETG, with ballooning parity. Ballooning-space mode structures in $A_\parallel$ (normalized to $B_0\rho_\mathrm{s}^2/a$) of the present MT are broader than those for the core MT in Ref. [9] and more comparable to spherical tokamak cases [33], extending to $|z| \approx 20\pi$. The mode width in Φ (normalized to $(T_{\mathrm{e}0}/e)\rho_\mathrm{s}/a$) matches that in $A_\parallel$, unlike in Refs. [9, 33], where Φ structures were broader than their $A_\parallel$ counterparts.

Different ETG branches, all strongly ballooned (e.g., the mode peaks at the outboard midplane), are separated by frequency discontinuities; as n is increased, modes branches are centered at lower ballooning angle but approximately constant $k_x \sim 20$. A dotted line shows $\gamma \propto k_y$ scaling: γ follows this trend, suggesting that turbulence from different scales may simultaneously affect transport [34].

Nonlinearly, focusing first on single-scale analyses, MT turbulence develops on ion scales, with the magnetic flutter flux Q_e^em peaking monochromatically at $n = 16$ (see Fig. 3, blue line), suggesting a moderate spectral shift or forward cascade relative to γ, unlike in the core MT case in Ref. [35]. In saturation, strong zonal Φ_z and zonal $A_{\parallel\mathrm{z}}$ are observed, dominating the turbulence; as ions are adiabatic and profiles fixed, the zonal-flow excitation is not a consequence of non-ambipolar transport but due to secondary instability [36].

A reduced nonlinear simulation is performed where the linear gradient drive is turned off and only the largest scales in x and y are retained, using as an initial condition the saturated

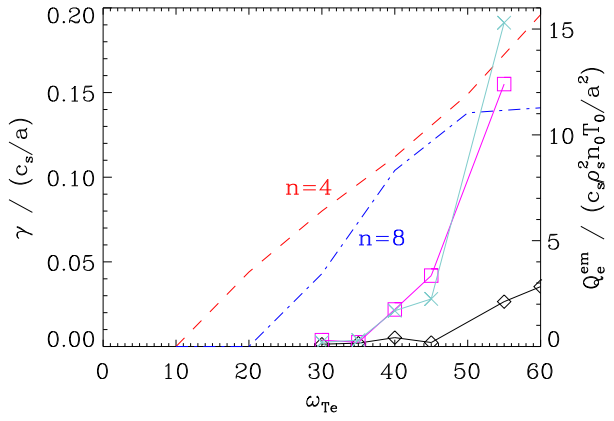

FIG. 4. Scaling of linear growth rates (red dashed line: $n = 4$, blue dash-dotted line: $n = 8$) and nonlinear heat flux (black solid line) with the electron temperature gradient. A clear shift in critical gradient is visible, from the linear threshold $\omega_{T\mathrm{e}} \approx 10$ to the nonlinear threshold $\omega_{T\mathrm{e}} \approx 45$. Pink squares show fluxes from simulations artificially removing $A_\parallel(k_y = 0)$, while additionally adding $\omega^{\mathrm{ext}}_{E\times B} = 0.5$ for the gray crosses: zonal fields clearly affect saturation, whereas fluxes are insensitive to $E\times B$ shear.

state of the full ion-scale simulation but rescaling the $n = 4$ mode (and not the zonal mode) by a factor of 10^{-10}. In the ensuing evolution, this mode grows at a rate approximately half of the linear growth rate of the original system. Thus, it can be concluded that tertiary growth may indeed influence the system but is subdominant to linear effects.

The nonlinear critical temperature gradient lies well above its linear counterpart, see Fig. 4, suggesting that $A_{\parallel\mathrm{z}}$ causes a nonlinear upshift akin to the Dimits shift [39]. $Q^{\mathrm{em}}_{\mathrm{e}}$ is not increased by artificial removal of Φ at the zonal mode $k_y = 0$; however, when instead removing the equivalent $A_\parallel(k_y = 0)$, one observes a significant flux increase and downshift of the nonlinear critical gradient, also in Fig. 4. This demonstrates that zonal-field-mediated energy transfer contributes to MT saturation—parallels to the zonal-flow-mediated transfer in Ref. [37] can be drawn. This finding is supported by an analysis of nonlinear energy transfer, which is almost exclusively channeled through (but not deposited in) the zonal mode. Conversely, electron temperature corrugations [38] do not modify the primary instability to a sufficient degree to affect saturation.

On electron scales (see Fig. 3, dotted red line), the electrostatic flux $Q^{\mathrm{es}}_{\mathrm{e}}$ reaches values comparable to MT flux; spectral pile-up can be seen at the largest scale (here, $n = 200$),

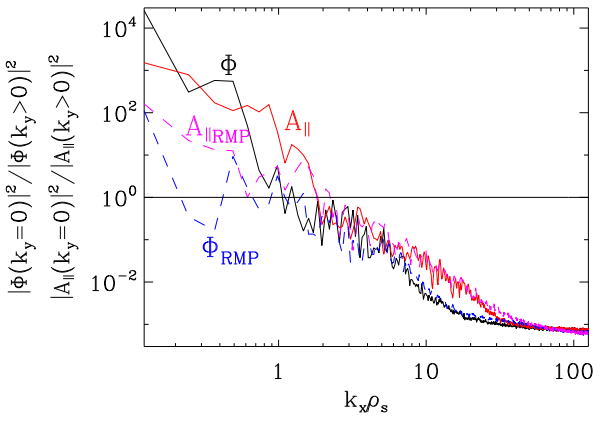

FIG. 5. Ratios of zonal to non-zonal amplitudes for Φ (black/blue) and $A_\parallel$ (red/pink). Solid lines correspond to no RMP, dashed lines include the RMP, leading to lower ratios.

but convergence checks show this does not affect the higher-n transport levels.

When computing all scales for a few ion transit times (over which the lowest n do not evolve significantly; this limitation is owed to the massive numerical expense), one key difference emerges relative to the single-scale situation: Q_e^{es} at high n is reduced by a factor of two, with a similar reduction in integrated electrostatic flux. The reason for this cross-scale interaction lies in zonal flow excitation by MT: these flows lower ETG-scale turbulence levels, a process which can be interpreted within the shearing paradigm [40] or the stable-mode paradigm [41, 42].

Conversely, while the ion-scale MT turbulence cannot fully react to electron-scale physics on simulated time scales, little such impact from small on large scales is expected. Contrary to the ETG-flow-based MT suppression reported in Ref. [17], the present MT instability is relatively insensitive to both linear Φ and nonlinear Φ_z saturation effects. Thus, the ETG cannot easily employ the route of $E\times B$ flow to regulate MT turbulence and fluxes. More direct evidence of this property is included in Fig. 4, where the inclusion of experimentally relevant levels of background $E\times B$ flow – as measured by the shearing rate $\omega_{E\times B}^{ext} = 0.5$ in standard frequency units – does not affect saturated MT heat flux levels.

Zonal flows also feature in explaining the effect of imposed RMP-type fluctuations. For this study, an experimentally relevant $B_x^{ext} = ik_y A_\parallel^{ext} \lesssim 6\times 10^{-4} B_0$ constant-in-time fluctuation at $n = 4$ with resonant, Gaussian shape in z was imposed at $k_x = 0$, specifically $A_\parallel(k_x = 0) \rightarrow A_\parallel(k_x = 0) + A_\parallel^{ext}\exp(-5z)^2$. An equivalent setup was used in Ref. [23],

where a successful comparison with experimental measurements of the RMP impact was obtained.

Notably, no RMP effect is observed on an instantaneous zonal field $A_{\parallel \mathrm{z}} = A_{\parallel}(k_y = 0)$, whereas the zonal flow residual [43] erodes promptly [18, 44] due to non-ambipolar charge loss. This mechanism equivalently affects the turbulent zonal-flow amplitude. However, given the comparative insensitivity of the MT turbulence to Φ_{z}, the impact on single-scale MT turbulent fluxes is limited, showing no interaction of the (also resonant) self-consistent $A_{\parallel}$ and $A_{\parallel}^{\mathrm{ext}}$. As expected, for the multi-scale case, adding the RMP and thereby diminishing the zonal flow amplitudes causes ETG fluxes to rise. Note that Ref. [19] has demonstrated that simulations with kinetic ions agree very well with the theory, which is based on static ions [18], equivalent to an adiabatic-ion response.

While the finding of a strong shift of amplitude from Φ_{z} to non-zonal Φ is evident for both large and intermediate scales in Fig. 5, a lesser but clear shift can be seen in the magnetic potential. However, the non-zonal $A_{\parallel}$ on which these numbers are based includes $A_{\parallel}^{\mathrm{ext}}$ (which cannot straightforwardly be subtracted due to shielding). Another observation is that, regardless of whether an RMP is present, small radial scales appear to rely to a far lesser degree on zonal flows or fields.

These findings can be contrasted with the weakly collisional core MT scenario presented in Ref. [9]. For the present work, an RMP identical to that described above is imposed for their parameter case of $\beta = 0.6\%$ and $R_0/L_{T\mathrm{e}} = 5$, yielding a $\sim 50\%$ increase in magnetic heat diffusivity, almost all of which is attributable to the self-consistent response rather than the direct RMP flutter transport. This result is not surprising, considering the MT mode studied in Ref. [9] relies on Φ for instability and saturation. A thorough classification of MT types will require inclusion of these disparate properties.

In summary, multi-scale interaction between microtearing and electron-temperature-gradient-driven turbulence in the tokamak pedestal reveals suppression of electron-scale flux by MT-borne large- and intermediate-scale zonal flows. Generalizability of this result relies on similarities in MT drive and collisionality regime, which are expected to match other pedestal scenarios. In particular, the reliance of the present flavor of MT on zonal fields rather than zonal flows for saturation is to be highlighted.

In terms of pedestal evolution, this reinforces the significance of MT turbulent transport while refining the picture with respect to ETG impact. However, as the inclusion of resonant

magnetic perturbations results in zonal-flow erosion and boosts ETG transport but leaves MT fluxes unaffected, ETG turbulence may require additional consideration in RMP discharges. The question how pellet injection and associated density profile steepening affects this picture is to be deferred for future investigation.

The authors wish to thank S. Mahajan, P.W. Terry, and Z.R. Williams for helpful discussions. This work was supported by U.S. DOE grant DE-FG02-04ER-54742 as well as Office of Fusion Energy Sciences Scientific Discovery through Advanced Computing (SciDAC) program, award DE-SC0018429. This research benefited from a collaboration made possible by the U.S.-Japan Joint Institute for Fusion Theory (JIFT) program.

[1] F. Wagner *et al.*, Phys. Rev. Lett. **49**, 1408 (1982)

[2] T.C. Hender *et al.*, Nucl. Fusion **32**, 2091 (1992)

[3] T.E. Evans *et al.*, Nucl. Fusion **45**, 595 (2005)

[4] H.R. Wilson, P.B. Snyder, R.L. Miller, and G.T.A. Huysmans, Phys. Plasmas **9**, 1277 (2002)

[5] D.R. Hatch, M. Kotschenreuther, S. Mahajan, P. Valanju, F. Jenko, D. Told, T. Görler, and S. Saarelma, Nucl. Fusion **56**, 104003 (2016)

[6] M. Kotschenreuther *et al.*, Nucl. Fusion **59**, 096001 (2019)

[7] W.M. Nevins, J. Candy, S. Cowley, T. Dannert, A. Dimits, W. Dorland, C. Estrada-Mila, G.W. Hammett, F. Jenko, M.J. Pueschel, and D.E. Shumaker, Phys. Plasmas **13**, 122306 (2006)

[8] R.D. Hazeltine, D. Dobrott, and T.S. Wang, Phys. Fluids **18**, 1778 (1975)

[9] H. Doerk, F. Jenko, M.J. Pueschel, and D.R. Hatch, Phys. Rev. Lett. **106**, 155003 (2011)

[10] W. Guttenfelder *et al.*, Phys. Rev. Lett. **106**, 155004 (2011)

[11] D.R. Hatch *et al.*, *Final Report for the FY19 FES Theory Performance Target*, United States (2019)

[12] D.R. Hatch *et al.*, *Microtearing modes as the source of magnetic fluctuations in the JET pedestal*, submitted to Nucl. Fusion

[13] J. Candy, R.E. Waltz, M.R. Fahey, and C. Holland, Plasma Phys. Control. Fusion **49**, 1209 (2007)

[14] T. Görler and F. Jenko, Phys. Rev. Lett. **100**, 185002 (2008)

[15] S. Maeyama, Y. Idomura, T.-H. Watanabe, M. Nakata, M. Yagi, N. Miyato, A. Ishizawa, and M. Nunami, Phys. Rev. Lett. **114**, 255002 (2015)

[16] M.R. Hardman, M. Barnes, C.M. Roach, and F.I. Parra, Plasma Phys. Control. Fusion **61**, 065025 (2019)

[17] S. Maeyama, T.-H. Watanabe, and A. Ishizawa, Phys. Rev. Lett. **119**, 195002 (2017)

[18] P.W. Terry, M.J. Pueschel, D. Carmody, and W.M. Nevins, Phys. Plasmas **20**, 112502 (2013)

[19] M.J. Pueschel, P.W. Terry, F. Jenko, D.R. Hatch, W.M. Nevins, T. Görler, and D. Told, Phys. Rev. Lett. **110**, 155005 (2013)

[20] D. Carmody, M.J. Pueschel, J.K. Anderson, and P.W. Terry, Phys. Plasmas **22**, 012504 (2015)

[21] Z.R. Williams, M.J. Pueschel, P.W. Terry, and T. Hauff, Phys. Plasmas **24**, 122309 (2017)

[22] S. Taimourzadeh, L. Shi, Z. Lin, R. Nazikian, I. Holod, and D. Spong, Nucl. Fusion **59**, 046005 (2019)

[23] Z.R. Williams, M.J. Pueschel, P.W. Terry, T. Nishizawa, D.M. Kriete, M.D. Nornberg, J.S. Sarff, G.R. McKee, D.M. Orlov, and S.H. Nogami, Nucl. Fusion **60**, 096004 (2020)

[24] J.D. Callen, R.J. Groebner, T.H. Osborne, J.M. Canik, L.W. Owen, A.Y. Pankin, T. Rafiq, T.D. Rognlien, and W.M. Stacey, Nucl. Fusion **50**, 064004 (2010)

[25] D.R. Hatch *et al.*, Nucl. Fusion **59**, 086056 (2019)

[26] X. Lapillonne, B.F. McMillan, T. Görler, S. Brunner, T. Dannert, F. Jenko, F. Merz, and L. Villard, Phys. Plasmas **17**, 112321 (2010)

[27] A.J. Brizard and T.S. Hahm, Rev. Mod. Phys. **79**, 421 (2007)

[28] F. Jenko and W. Dorland, Plasma Phys. Control. Fusion **43**, A141 (2001)

[29] M.J. Pueschel, F. Jenko, D. Told, and J. Büchner, Phys. Plasmas **18**, 112102 (2011)

[30] M.J. Pueschel, T. Dannert, and F. Jenko, Comp. Phys. Commun. **181**, 1428 (2010)

[31] A.B. Hassam, Phys. Fluids **23**, 2493 (1980)

[32] J.F. Drake, N.T. Gladd, C.S. Liu, and C.L. Chang, Phys. Rev. Lett. **44**, 994 (1980)

[33] D.J. Applegate, C.M. Roach, J.W. Connor, S.C. Cowley, W. Dorland, R.J. Hastie, and N. Joiner, Plasma Phys. Control. Fusion **49**, 1113 (2007)

[34] G.M. Staebler, J. Candy, N.T. Howard, and C. Holland, Phys. Plasmas**23**, 062518 (2016)

[35] H. Doerk, F. Jenko, T. Görler, D. Told, M.J. Pueschel, and D.R. Hatch, Phys. Plasmas **19**, 055907 (2012)

[36] S.C. Cowley, R.M. Kulsrud, and R. Sudan, Phys. Fluids B **3**, 2767 (1991)

[37] M. Nakata, T.-H. Watanabe, and H. Sugama, Phys. Plasmas **19**, 022303 (2012)

[38] M.J. Pueschel, T. Görler, F. Jenko, D.R. Hatch, and A.J. Cianciara, Phys. Plasmas **20**, 102308 (2013)

[39] A.M. Dimits *et al.*, Phys. Plasmas **7**, 969 (2000)

[40] P.H. Diamond, S.-I. Itoh, K. Itoh, and T.S. Hahm, Plasma Phys. Control. Fusion **47**, R35 (2005)

[41] K.D. Makwana, P.W. Terry, M.J. Pueschel, and D.R. Hatch, Phys. Rev. Lett. **112**, 095002 (2014)

[42] P.W. Terry, B.J. Faber, C.C. Hegna, V.V. Mirnov, M.J. Pueschel, and G.G. Whelan, Phys. Plasmas **25**, 012308 (2018)

[43] M.N. Rosenbluth and F.L. Hinton, Phys. Rev. Lett. **80**, 724 (1998)

[44] M.J. Pueschel, D.R. Hatch, T. Görler, W.M. Nevins, F. Jenko, P.W. Terry, and D. Told, Phys. Plasmas **20**, 102301 (2013)